BM-D-11-00863 – Revision 1. Original

Shape optimization of stress concentration-free lattice for self-expandable Nitinol stent-grafts

Ehsan Masoumi Khalil Abad: PhD candidate, Mechanical Engineering Department, McGill University, Montreal, Quebec, Canada. Email: ehsan.masoumikhalilabad@mail.mcgill.ca

Damiano Pasini: Associate Professor, Mechanical Engineering Department, McGill University, Montreal, Quebec, Canada. Email: damiano.pasini@mcgill.ca

Renzo Cecere: Associate Professor in Surgery, McGill University Health Center, McGill University, Montreal, Quebec, Canada. Email: renzo.cecere@muhc.mcgill.ca

Correspond Author: Damiano Pasini

Address: Room 372, Macdonald Engineering Building, 817 Sherbrooke street west, Montreal, Quebec, Canada, H3A 2K6, Tel: +1-514-398-6295, Fax: +1-514-398-7365

Number of words (introduction through discussion): 3764

Abstract:

In a mechanical component, stress-concentration is one of the factors contributing to reduce fatigue life. This paper presents a design methodology based on shape optimization to improve the fatigue safety factor and increase the radial stiffness of Nitinol self-expandable stent-grafts. A two dimensional lattice free of stress concentrators is proposed for the synthesis of a stent with smooth cell shapes. Design optimization is systematically applied to minimize the curvature and reduce the bending strain of the elements defining the lattice cells. A novel cell geometry with improved fatigue life and radial supportive force is introduced for Nitinol self-expandable stent-grafts used for treating abdominal aortic aneurism. A parametric study comparing the optimized stent-graft to recent stent designs demonstrates that the former exhibits a superior anchoring performance and a reduction of the risk of fatigue failure.

1. Introduction

Intravascular stents are primarily used to open and scaffold tubular passages or lumens such as blood vessels, biliary ducts and the esophagus (Duerig et al. 1999). They usually consist of expandable lattice meshes that can deploy and hold endovascular grafts, arterial endoprosthesis and self-expanding heart valve implants. Figure 1 (a-e) shows recent commercial applications of stent devices, which are designed to deploy into the body by minimally invasive percutaneous intervention (Kleinstreuer et al. 2008; Rose et al. 2001; Vergnat et al. 2009; Webb 2008).

Depending on the stent application, stents should address multiple functional requirements and often conflicting objectives. For example, bare metal stents used for opening the occluded arteries should provide a combination of high radial force and axial flexibility in order to keep the artery open, prevent stent migration, conform to the curved blood vessels, and flex during the body movement (Cheng et al. 2006). Stents used as prostheses of aortic valve are required to provide high radial strength to expand and to exclude the calcified leaflets and to avoid recoil (Grube et al. 2006). In endovascular repair for abdominal aortic aneurisms (*AAAs*), the structure of a stent-graft should provide sufficiently high radial force to prevent graft migration and blood leakage into the aneurysm cavity (Kleinstreuer and Li 2006; Kleinstreuer et al. 2008).

Since 1990, an ever increasing demand for endovascular stents has led to significant advancements in the field of analysis, modelling and design of stent structures. Restenosis rate, vessel patency, cloth formation, stent migrations, stent collapse, stent positioning and stent expansion behaviour are common concerns that have attracted the attention of several researchers (Chua et al. 2002; Duerig et al. 1999; Kleinstreuer et al. 2008; Martin and Boyle 2010; Petrini et al. 2004; Migliavacca et al. 2002; Lim et al. 2008; Lally et al. 2005; Timmins et

al. 2007; Bedoya et al. 2006; Wang and Masood 2006; Flueckiger et al. 1994). These studies have shown that besides mechanical and biological factors, the geometry and typology of a stent is a crucial aspect that governs the device function and its performance.

Shape and size, as well as the thickness of a lattice cell, are geometric variables that can be tailored to improve the mechanical performance of a stent structures, such as its fatigue life, axial flexibility and radial stiffness. Design optimization can be used to find the values of these variables that best optimize one or more performance metrics of a stent device. So far, however, the synthesis of stents through systematic design optimization has received minor attention. For example, Figure 1(f) shows the structural geometry of a recent stent consisting of a 2D lattice of closed cells (Zhi et al. 2008). At the blending points between the arcs and the linear segments of each cell, the curvature has a discontinuity that acts as a stress concentrator (Neuber 1967). In ten years life, a stent can undergo nearly four hundred millions of cycles mainly because of pulsating blood pressure and body movement. Such a cyclic load drastically amplifies the effect of stress concentration that eventually reduces the fatigue life of the stent. The issue of reducing the level of stress concentration, a common concern in mechanical design, motivates this paper. Due to the existence of several stent applications, each entailing the fulfillment of specific requirements, this study focuses on stent grafts used for treating abdominal aortic aneurism. The success of these stent grafts is often undermined by stent fatigue, graft migration, and blood leakage into the aneurysm cavity (Kleinstreuer and Li 2006; Li and Kleinstreuer 2005). Two strategies can be adopted to reduce these risks: i) stiffen the stent in the radial direction to reduce endovascular leakage and device migration; ii) increase fatigue life to reduce the level of the alternating strain generated by a pulsating blood pressure.

We present in this paper a design strategy, which is expressed in the form of mathematical rigour and design optimization, to synthesize a stress-concentration free two-dimensional lattice. The results are compared with those obtained by (Kleinstreuer et al. 2008), and are discussed through a parametric study to investigate the effect of selected geometric parameters, e.g. tube thickness, strut width, and number of lattice cells, on stent fatigue life and radial supportive force.

2. Shape synthesis of lattice geometry

2.1. Lattice cells with smooth shape elements

In a 10 years expected design life, stents and stent grafts undergo nearly 4×10^8 cycles of alternating forces arising from pulsating blood pressure and body movement (Pelton et al. 2008). Such a loading condition could potentially lead to fatigue failure, especially for stents grafts made of Nitinol, which has a lower resistance to fatigue crack growth in comparison to other metals(Pelton et al. 2008; Stankiewicz et al. 2007; Robertson et al. 2007; Robertson and Ritchie 2007; McKelvey and Ritchie 2001).

It is well known that stress concentration can reduce the fatigue resistance of a mechanical part. Stress concentration can occur in the presence of abrupt changes in geometry. Notches, circular fillets, grooves are common examples of stress concentrators. Their role is to perturb locally the stress flow each time there is a curvature discontinuity in the primitives defining the geometry of a structural element (Neuber 1961a). Their detrimental impact has been studied in the literature (Pedersen 2007; Neuber 1961a; Pilkey 2007; Williams 1952; Dunn et al. 1997) , starting from the seminal work of Neuber, who first developed a theory of notch stresses with reference to the form and the material of an element. Neuber showed that the stress concentration factor increases by reducing the radius of the curvature of the boundary profile of a structure (Neuber 1961a) . In

addition, (Neuber 1961b) showed that under pure shear loading condition the elastic stress concentration, K_t , is equal to the multiplication of the notch stress concentration factor, K_ε , and the strain concentration factor , K_σ . Later studies performed by (Topper et al. 1969; Walker 1970) showed that this relationship is valid also for other static and cyclic stress states. More recently, researchers devoted their attention to the design aspects involving strategies to reduce the effect of stress concentrators. It has been shown that by controlling the curvature of a fillet, the stress flow might be smoothed to decrease the stress values. For example, (Desrochers 2008) looked at how to optimize the shape profile of an element to reduce its stress regime under static condition. (Waldman et al. 2001) studied the fatigue of shaft shoulders under tension and bending loading; he showed that an optimized-shape fillet can provide 23% higher fatigue life than a circular-shape fillet.

Figure 1(f) shows the geometry of a common stent (Zhi et al. 2008). The mesh elements are filleted at the blending points, where their tangent changes continuously. The stent, however, exhibits curvature discontinuity at each blending point which triggers stress concentration and might accelerate its fatigue failure. To remove the occurrence of geometry discontinuity in a stent, we propose here to synthesize the unit cell of the lattice with curves that are continuous in their curvature; this implies that the boundaries shaping each cell should be G^2-continuous (Teng et al. 2008). Through the formulation of a structural optimization problem explained in the next section, we first impose that each cell members be G^2- continuous at the blending points with adjacent elements and then be *as straight as possible*, i.e. with the smallest possible curvature, to reduce the high bending strains caused by curved cell members.

Figure 2 shows the unit cell of the lattice stent consisting of G^2-continous curves. The unit cell is repeated in a planar sheet to form the lattice, which is then folded into a cylindrical surface. The

lattice cylinder is described by n_c cells in the circumferential direction and n_l cell rows in the longitudinal direction. The tube thickness and strut width are respectively t and w, and we assume that the stent has a total length of 100mm and a non-shrunk diameter of 30mm (Kleinstreuer et al. 2008). Next sections describe how the geometry of the lattice cells for a Nitinol stent-graft can be optimized to improve fatigue life.

2.2. Mathematical formulation of the optimization problem

The design method is proposed to find smooth lattice cell topologies based on the synthesis of structural members with G^2-continuous curves that have minimum root mean square, or *rms*, value of the curvature (Teng et al. 2008). The first stage of the shape synthesis involves geometry optimization, in which only the *rms* value of the curvature of the cell elements is minimized. At this step, the material properties of Nitinol are ignored. The second stage entails the structural optimization of the unit cell and requires accounting also for the attributes and stress-strain curve of the material.

The shape synthesis of the lattice strut is stated as follows: *under given end conditions, find a boundary-curve Γ that connects two given end points A and B of the cell strut as smoothly as possible and with a G^2-continuous curve*. By parametrizing the cell strut boundary-curve Γ as a function of the arc-length s along the strut, we can formulate the optimization problem as(Teng et al. 2008):

$$J(\Gamma) = \frac{1}{L}\int_A^B \kappa^2 ds \;\rightarrow\; \min_{\Gamma(s)} \qquad (1)$$

where $\sqrt{\mathrm{J}}$ is the *rms* value of the curvature of a cell member boundary-curve, L is the member length, A and B are its end-points, and ds is the arc-length along the member, starting from *0* at point *A*, as shown in figure 2 (b). The member boundary-curve is subjected to four constraints

at each end-point. Two constraints define the end-points coordinates, while the other two set the tangent and curvature of the curve at these points.

Equation 1 can be treated as a problem of mathematical programming by means of non-parametric cubic splines (Spath 1995). Hence, each boundary curve is discretized by $n+2$ supporting points $\{P_k\}_0^{n+1}$ that are defined by $P_k(\rho_k,\theta_k)$ in a polar coordinate system. As shown in figure 2(b), P_k is a generic point of the curve; $P_0=A$ and $P_{n+1}=B$, where $A(\rho_A,\theta_A)$, and $B(\rho_B,\theta_B)$ are two end-points of the boundary-curve of each cell element. Moreover, if we assume that the discrete points are located at constant tangential intervals, the tangential increment will be:

$$\Delta\theta=\frac{\theta_B-\theta_A}{n+1} \qquad (2)$$

A cubic spline, $\rho(\theta)$, between two consecutive supporting points P_k and P_{k+1} can be defined as:

$$\rho(\theta)=A_k(\theta-\theta_k)^3+B_k(\theta-\theta_k)^2+C_k(\theta-\theta_k)^2+D_k \qquad (3)$$

The radial coordinates, the first and second derivatives of the cubic splines at the k^{th} supporting point, ρ,ρ' and ρ'', respectively, are represented by the following three vectors:

$$\begin{aligned}\boldsymbol{\rho}&=[\rho_0,\rho_1,....\rho_n,\rho_{n+1}]^T\\ \boldsymbol{\rho}'&=[\rho_0',\rho_1',....\rho_n',\rho_{n+1}']^T\\ \boldsymbol{\rho}''&=[\rho_0'',\rho_1'',....\rho_n'',\rho_{n+1}'']^T\end{aligned} \qquad (4)$$

Imposing the G^2-continuity condition results in the following linear relationships between ρ and ρ'' and between ρ and ρ':

$$\boldsymbol{A\rho''}=6\boldsymbol{C\rho} \text{ and } \boldsymbol{P\rho'}=\boldsymbol{Q\rho} \qquad (5)$$

where $\boldsymbol{A}$, $\boldsymbol{C}$, $\boldsymbol{P}$, and $\boldsymbol{Q}$ are defined in appendix A (Teng et al. 2008). Furthermore, $\rho_0=\rho_A$ and $\rho_{n+1}=\rho_B$ are known from a given parameter vector of the cell. Now, if $\boldsymbol{x}$ is the vector of the design variables, defined as

$$\boldsymbol{x}=[\rho_1,....\rho_n]^T \qquad (6)$$

the discretized shape optimization problem can be written as (Teng et al. 2008)

$$z(\boldsymbol{x})=\frac{1}{n}\sum_{1}^{n} w_k\kappa_k^2 \quad \rightarrow \quad \min_{\boldsymbol{x}} \qquad (7)$$

Where w_k is the weighting coefficient of point k^{th} defined at each supporting point, and representing the contribution of each point on the curvature of the optimum curve. Furthermore, the curvature at each point P_k is given by:

$$\kappa_k=\frac{\rho_k^2+2(\rho_k')^2-\rho_k\rho_k''}{(\rho_k^2+(\rho_k')^2)^{3/2}} \qquad (8)$$

Discretizing the objective function (eq. (7)) and applying the constraints at the end points of the boundary curve, allow solving the problem with mathematical programming. The required number of supporting points depends on the geometric boundary conditions. After performing a sensitivity analysis, the figure of 100 supporting points has been selected for the boundary curves.

To solve the optimization problem, we used a sequential quadratic programming algorithm employing orthogonal decomposition algorithm. The details of this method can be found in the work of (Teng and Angeles 2001). Furthermore for comparison purposes, we tested the genetic algorithm and found the same results.

As written at the beginning of this section, the first stage of geometry optimization assumes equal weighting coefficients, i.e. $1/n$, to find a geometrically optimum boundary of the unit cell. This result is then further optimized at a second stage, in which the stress and strain regimes are taken into account. In this case, the expressions of the weighting coefficients, w_k, (equation (7)) are considered as a function of the strain regime obtained iteratively at each *FEA* iteration. We consider strain, rather than stress as used by (Teng et al. 2008), since the plateau region of the Nitinol stress-strain curve (Figure 3), which corresponds to the stress induced phase transformation from the austensite to the martensite state, is much more sensitive to strain changes. This has a strong impact on the alternating strain and thus on the fatigue life Nitinol. The weight coefficients are therefore not uniform along the cell strut boundary-curve and they are defined as:

$$w_k = \frac{\bar{\varepsilon}_k}{\bar{\varepsilon}_T} \qquad (9)$$

where $\bar{\varepsilon}_k$ and $\bar{\varepsilon}_T$ are, respectively, the *rms* value of the von Mises strain at the k^{th} supporting point of the profile curve, and the *rms* value of the strain over the whole cell element of the stent and are defined as:

$$\bar{\varepsilon}_T = \sqrt{\frac{1}{m}\sum_{i=1}^{m}\varepsilon_i^2} \qquad (10)$$

$$\bar{\varepsilon}_k = \sqrt{\frac{1}{\mu_k}\sum_{i=1}^{\mu_k}\varepsilon_{ki}^2}\ , \quad \mu_k = \frac{m}{50} \qquad (11)$$

where m is the total number of nodes in the FE model, ε_i is the von Mises strain at ith node and ε_{ki} is the von Mises strain of the μ_k nodes (2% of the total nodes of FE model), which are

relatively closer to the kth supporting point. The structural optimization algorithm is set to end when the reduction in the maximum strain value is smaller than 0.1%. Numerical modeling

2.2.1. *Finite element modeling*

The stent geometry is automatically synthesized through an in-house MATLAB subroutine, which is coupled to ANSYS to build, mesh, and solve the *3D* model of the stent. Here, only the stent rows in contact with the aneurism neck are examined due to their importance for stent-graft migration and fatigue life (Kleinstreuer et al. 2008). Usually, a stent consists of a set of separate rows that are sutured on the graft fabric. Between rows, there is a gap in the axial direction to allow a relative movement of the stent rows and to increase the axial flexibility of the stent. In the sealing section located at the two distal rows of the stent-graft, the stent does not gain its original size and the graft material is not in tension. Since the stiffness of the graft material is very low, the effect of the connectivity of the rows in the sealing section can be neglected (Kleinstreuer et al (2008)).

Because of symmetry in both geometry and loading, only ¼ of one cell is modeled. Symmetric boundary conditions are applied at the planes of symmetry. To mesh the stent elements of the lattice cell, a 3D eight-node element type, *SOLID 185*, is selected. The arterial wall is modeled as a cylinder and meshed by a twenty-node element type, *SOLID 95*. A mesh sensitivity test is also performed to ensure the independency of the results from the mesh size.

2.2.2. *Material model*

Nitinol is a pseudo-elastic material extensively used in biomedical devices for its bio-compatibility, shape memory property besides outstanding ability to withstand severe deformation. Figure 3 is a schematic view of the stress-strain curve of Nitinol at a given

temperature. To model the super-elasticity characteristics of Nitinol, here we use the constitutive model presented by (Auricchio 1995). Figure 3(b) shows the material properties of Nitinol used in this study.

The structure of the artery wall is assumed to be incompressible with a Young's modulus of 1.2MPa and a Poisson's ratio of 0.495, as prescribed by FDA protocols (ASTM 2007).

2.2.3. *Loading conditions*

a. Shrinking loading

For delivery purposes, the stent-graft with outer diameter of 30mm must be first shrunk to fit into the 24F delivery sheath and then, when deployed, must regain its original shape. We model the shrinking manoeuvre by applying a radial displacement to a rigid movable surface, which is in frictionless contact with the strut outer surface. The graft material is assumed to have a negligible effect on the overall behaviour of the stent in the sealing section; thus the graft is not considered in the model.

b. Sealing loading

The stent should be anchored to the neck artery of the abdominal aortic aneurism (*AAA*) after its release from the deployment system. The anchoring force should be sufficiently high to prevent the stent-graft migration. In this study, the stent deployment is modeled in two steps. First, the stent is shrunk to a diameter close to the artery interior wall by using rigid contact surface. Second, the stent expanded to reach an equilibrium radius in contact with the artery wall by gently removing the contact surface of the rigid body. The diastolic and systolic blood pressures are modeled as constant pressures applied to the inner surface of the artery wall.

3. Results

Figure 2(c) shows the results of minimizing the curvature of the inner boundary-profile for the *E* lattice cell. Figure 4 shows the views of the structurally optimized stents.

Figures 5(a) illustrate the von Mises strain distribution in the shrunk stent. It can be seen that maximum strain level is below the 12% allowable threshold strain limit of Nitinol (Kleinstreuer et al. 2008). It shows that the stent can shrunk without fracture. The distribution of the first principal strain in the deployed stents is shown in figure 5(b). Table 1 shows the performance of the proposed design in comparison with the *R* stent (Kleinstreuer et al. 2008). We note that the requirement used for comparison is the area of the R stent in contact with the artery; this area is assumed to be equal to the area of the E stent. As explained later in the discussion, the deployment constraint imposes a maximum on the allowable number of cells in the circumferential direction. For a given surface area requirement, we select the strut width as design variable and we fix as design parameters: 1) the number *of cells in the longitudinal direction* so as the stents have equal share of pressure on the artery wall at each row; 2) *the stent thickness*, as its effect on the blood flow and hemodynamic properties is significant. Table 1 shows that the proposed *E* stent has 69.1% higher fatigue safety factor[1] and 82.4% larger radial supportive force per unit of stent area. Figures 5(c) show the von Mises stress distribution induced in the artery wall after graft deployment. The stress level in the artery wall is below 0.67MPa, the elastic limit of the artery (Raghavan et al. 1996). However, compared to the *R* stent, the level of von Mises stress induced in the artery wall exhibits a 32.4% increase. This

---

[1] Fatigue safety factor $= \dfrac{\text{Nitinol alternating strain limit } (\varepsilon_{\text{all}})}{\text{Alternating strain of stent } (\varepsilon_{\text{alt}})}$ where $\varepsilon_{\text{all}} = 0.4\%$ (Pelton et al. 2004) and $\varepsilon_{\text{all}} = 0.5(strain \;\; at \;\; 150mmHg - strain \;\; at \;\; 150mmHg)$

stress level might reduce over time but it should be below the allowable elastic limit of the artery wall after stent insertion.

Figure 6 illustrates the radial supportive force as a function of the outer diameter for *E* stent in comparison with the *R* stent for a prescribed stent area and tube thickness. For a 2mm constant radial displacement, the proposed *E* cell design provides 165% increase in the supportive radial force.

4. Discussion and Concluding Remarks

To discuss the effect of the changes in the geometry of the optimized stent geometry, we have performed a parametric study that assesses the role of n_c, n_l, t, and w on i) the deployed stent supportive radial force under 100 mmHg blood pressure; ii) stent fatigue safety factor; and iii) stent area. Figure 7 summarizes the results. As can been seen, the application of the proposed methodology enables to find lattice design with higher fatigue safety factor and an improved radial supportive force. In particular, for a 25% increase of n_c, n_l, t, and w, the radial supportive force increases respectively by 1.4%, 18.55%, 7.39%, and 2.11%. The fatigue safety factor improves by 49.7%, 45.5%, 50.7%, and 41.6%. The stent area also increases of 14.7%, 14.8%, 16.1% and 0%. The above benefits come along with a side-effect, i.e. an increase of the level of von Mises stress induced in the artery wall. This is mainly caused by a higher radial supportive force applied by the sharp edges of the stent struts in contact with the artery wall. However, it should be noted that despite the higher stress level in the artery wall, the contact stress is distributed more uniformly around the artery wall. Furthermore, this stress level can be easily reduced by rounding the sharp fillet of the strut edges of the stent in contact with the artery.

The results of the parametric study show that to obtain a shrinkable stent an upper limit is required on the number of cells in the circumferential direction. For example, Figures 7 (a-c) show that for a stent with n_l =10, t=0.28mm, w=0.45mm, only values of n_c less than 10 enable the stent to can be shrunk without fracture.

The impact of the number of cells in the circumferential direction, n_c, is illustrated in Figures 7(a-c). Whereas the supportive radial force of the stent is not affected, the stent area shows a rapid linear increase. The stent fatigue safety factor, on the other hand, decreases if n_c reduces. Therefore, higher values of n_c should be chosen while respecting the deployment constraint (Fig 7(a)). It is worthy to mention, also, that reducing n_c might increase the stress level in the artery wall.

Figures 7(d-f) illustrate the influence of the number of cells, n_l, in the longitudinal direction on stent performance. By increasing n_l for a given arterial length, the share of each row in supporting the arterial radial load decreases that reduces the level of radial supportive force (Fig. 8(d)). In addition, the stiffness of the stent increases by shortening the length of each cell row. This outcome improves the stent fatigue safety factor by reducing the level of alternating strain.

Figures 7(g) and 8(j) show that thickening the strut and width is beneficial for both stent radial stiffness and radial supportive force. Besides these gains, a stiffer stent would be also more resistant to the deformation imposed by a pulsatile pressure, thereby reducing the alternating strain experienced by its members. This is observed in Figures 7(h) and 7(k), where the fatigue safety factor increases linearly with w and t. On the other hand, Figure 7(i) shows that the stent area is not affected by any change of the stent thickness as opposed to the trend observed by varying n_c, n_l, w in Figures 7(c), (f), and (l).

The result of Figures 7(g), however, should be taken with a caution. A thicker strut will cause a higher contact stress in the artery wall. Furthermore, blood flow in proximity with the artery wall and stent struts will affect the selection of the strut thickness. These issues should be determined through multi-disciplinary analysis and optimization involving both computational fluid dynamics and structural analysis.

The methodology proposed in this paper can be extended to synthesize the geometry of other types of stents, e.g. superficial femoral artery stents, to meet prescribed design objectives imposed by the specific application. The work is part of ongoing research; our current and future efforts target two main research venues, as describe below.

- *Design optimization.* As shown by the results of the parametric study, stent radial supportive force, fatigue failure safety factor, and stress level in the artery wall often have conflicting outcomes. An improvement of one will penalize the other. It is, thus, necessary to formulate the shape synthesis of the lattice cell within a multi-objective optimization framework (Messac et al. 2003), which would be capable of providing trade-off solutions among conflicting objective functions, such as those identified in this discussion.
- Fracture mechanics approach. In this paper, stent design for fatigue life was tackled by minimizing the occurrence of stress concentration due to geometric discontinuity. This method can be complemented by integrating a fracture mechanics approach, which is based on the design guidelines for fatigue design of Nitinol devices (Robertson and Ritchie 2007; Robertson and Ritchie 2008; Stankiewicz et al. 2007).

Conflict of interest Statement

There are no conflicts of interest.

Acknowledgments

This work is funded by the Natural Sciences and Engineering Research Council of Canada (NSERC). The authors thank MD O. Steinmetz, chief of service, Division of Vascular Surgery (McGill University Health center), for providing useful insight into the endovascular techniques used to repair aortic aneurysms.

ASTM, I., 2007. Standard test methods for in vitro pulsatile durability testing of vascular stents. ASTM Standard F2477. West Conshohocken, PA

Auricchio, F., 1995. Shape Memory Alloys: Applications, Micromechanics, Macromodeling and Numerical Simulations. University of California at Berkely,

Bedoya, J., Meyer, C.A., Timmins, L.H., Moreno, M.R., Moore, J.J.E., 2006. Effects of Stent Design Parameters on Normal Artery Wall Mechanics. Journal of Biomechanical Engineering 128 (5), 757-765.

Cheng, C.P., Wilson, N.M., Hallett, R.L., Herfkens, R.J., Taylor, C.A., 2006. In Vivo MR Angiographic Quantification of Axial and Twisting Deformations of the Superficial Femoral Artery Resulting from Maximum Hip and Knee Flexion. Journal of vascular and interventional radiology : JVIR 17 (6), 979-987.

Chua, S.N.D., Mac Donald, B.J., Hashmi, M.S.J., 2002. Finite-element simulation of stent expansion. Journal of Materials Processing Technology 120 (1-3), 335-340.

Desrochers, S., 2008. Optimum design of simplicial uniaxial accelerometers. McGill University,

Duerig, T., Pelton, A., Stöckel, D., 1999. An overview of nitinol medical applications. Materials Science and Engineering A 273-275, 149-160.

Dunn, M.L., Suwito, W., Cunningham, S., 1997. Stress intensities at notch singularities. Engineering Fracture Mechanics 57 (4), 417-430.

Flueckiger, F., Sternthal, H., Klein, G.E., Aschauer, M., Szolar, D., Kleinhappl, G., 1994. Strength, Elasticity, and Plasticity of Expandable Metal Stents: In Vitro Studies with Three Types of Stress. Journal of Vascular and Interventional Radiology 5 (5), 745-750.

Grube, E., Laborde, J.C., Gerckens, U., Felderhoff, T., Sauren, B., Buellesfeld, L., Mueller, R., Menichelli, M., Schmidt, T., Zickmann, B., Iversen, S., Stone, G.W., 2006. Percutaneous Implantation of the CoreValve Self-Expanding Valve Prosthesis in High-Risk Patients With Aortic Valve Disease. Circulation 114 (15), 1616-1624.

Kleinstreuer, C., Li, Z., 2006. Analysis and computer program for rupture-risk prediction of abdominal aortic aneurysms. BioMedical Engineering Online 5 (1), 19.

Kleinstreuer, C., Li, Z., Basciano, C.A., Seelecke, S., Farber, M.A., 2008. Computational mechanics of Nitinol stent grafts. Journal of Biomechanics 41 (11), 2370-2378.

Lally, C., Dolan, F., Prendergast, P.J., 2005. Cardiovascular stent design and vessel stresses: a finite element analysis. Journal of Biomechanics 38 (8), 1574-1581.

Li, Z., Kleinstreuer, C., 2005. Blood flow and structure interactions in a stented abdominal aortic aneurysm model. Medical Engineering & Physics 27 (5), 369-382.

Lim, D., Cho, S.-K., Park, W.-P., Kristensson, A., Ko, J.-Y., Al-Hassani, S., Kim, H.-S., 2008. Suggestion of Potential Stent Design Parameters to Reduce Restenosis Risk driven by

Foreshortening or Dogboning due to Non-uniform Balloon-Stent Expansion. Annals of Biomedical Engineering 36 (7), 1118-1129.
Martin, D., Boyle, F.J., 2010. Computational structural modelling of coronary stent deployment: a review. Computer Methods in Biomechanics and Biomedical Engineering.
McKelvey, A.L., Ritchie, R.O., 2001. Fatigue-crack Growth Behavior in the Superelastic and Shape-memory Alloy Nitinol. Metallurgical and Materials Transactions A: Physical Metallurgy and Materials Science 32 (Compendex), 731-743.
Messac, A., Ismail-Yahaya, A., Mattson, C., 2003. The Normalized Normal Constraint Method for Generating the Pareto Frontier. Structural and Multidisciplinary Optimization 25 (2), 86-98.
Migliavacca, F., Petrini, L., Colombo, M., Auricchio, F., Pietrabissa, R., 2002. Mechanical behavior of coronary stents investigated through the finite element method. Journal of Biomechanics 35 (6), 803-811.
Neuber, H., 1961a. Theory of notch stresses: Principles for Exact Calculation of Strength with Reference to Structural Form and Material. 2nd edn. United States Atomic Energy Commission, Washington
Neuber, H., 1961b. Theory of Stress Concentration for Shear Strained Prismatic Bodies with Arbitrary Nonlinear Stress-Strain Law. Journal of Applied Mechanics,Transactions of the ASME 28, 554.
Neuber, H., 1967. Theory of notch stresses: Principles for Exact Calculation of Strength with Reference to Structural Form and Material. 2nd edn. United States Atomic Energy Commission, Washington
Pedersen, P., Year. Published Some Benchmarks for Optimized Shapes with Stress Concentration. In Proceeding of the, 2007.
Pelton, A.R., Gong, X.Y., Duerig, T., Year. Published Fatigue testing of diamond-shaped specimens. In Proceeding of the, 2004. Asm Intl, p 199.
Pelton, A.R., Schroeder, V., Mitchell, M.R., Gong, X.-Y., Barney, M., Robertson, S.W., 2008. Fatigue and Durability of Nitinol Stents. Journal of the Mechanical Behavior of Biomedical Materials 1 (2), 153-164.
Petrini, L., Migliavacca, F., Auricchio, F., Dubini, G., 2004. Numerical Investigation of the Intravascular Coronary Stent Flexibility. Journal of Biomechanics 37 (4), 495-501.
Pilkey, W.D., 2007. Frontmatter. In, Peterson's Stress Concentration Factors. John Wiley & Sons, Inc., pp. i-xxxii.
Raghavan, M., Webster, M., Vorp, D., 1996. Ex vivo biomechanical behavior of abdominal aortic aneurysm: Assessment using a new mathematical model. Annals of Biomedical Engineering 24 (5), 573-582.
Robertson, S.W., Mehta, A., Pelton, A.R., Ritchie, R.O., 2007. Evolution of Crack-tipTransformation Zones in Superelastic Nitinol Subjected to in Situ Fatigue: A Fracture Mechanics and Synchrotron X-ray Microdiffraction Analysis. Acta Materialia 55 (18), 6198-6207.
Robertson, S.W., Ritchie, R.O., 2007. In Vitro Fatigue-crack Growth and Fracture Toughness Behavior of Thin-walled Superelastic Nitinol Tube for Endovascular Stents: A Basis for Defining the Effect of Crack-like Defects. Biomaterials 28 (4), 700-709.
Robertson, S.W., Ritchie, R.O., 2008. A fracture-mechanics-based approach to fracture control in biomedical devices manufactured from superelastic Nitinol tube. Journal of Biomedical Materials Research Part B: Applied Biomaterials 84B (1), 26-33.
Rose, J.D.G., Pimpalwar, S., Jackson, R.W., 2001. A new stent-graft for transjugular intrahepatic portosystemic shunts. Br J Radiol 74 (886), 908-912.
Spath, H., 1995. One Dimensional Spline Interpolation Algorithms. A K Peters, Wellesley, Mass
Stankiewicz, J., Robertson, S., Ritchie, R., 2007. Fatigue-crack growth properties of thin-walled superelastic austenitic Nitinol tube for endovascular stents. Journal of Biomedical Materials Research Part A 81A (3), 685-691.
Teng, C.P., Bai, S., Angeles, J., 2008. Shape Synthesis in Mechanical Design. Acta Polytechnica 47 (6), 56-62.

Timmins, L., Moreno, M., Meyer, C., Criscione, J., Rachev, A., Moore, J., 2007. Stented artery biomechanics and device design optimization. Medical and Biological Engineering and Computing 45 (5), 505-513.
Topper, T., Wetzel, R., Morrow, J.D., 1969. Neubers Rule Applied to Fatigue of Notched Specimens. J MATER 4 (1), 200-209.
Vergnat, M., Henaine, R., Kalejs, M., Bommeli, S., Ferrari, E., Obadia, J.-F., Von Segesser, L.K., 2009. A new self-expanding aortic stent valve with annular fixation: in vitro haemodynamic assessment. Eur J Cardiothorac Surg 35 (6), 970-976.
Waldman, W., Heller, M., Chen, G., 2001. Optimal free-form shapes for shoulder fillets in flat plates under tension and bending. International Journal of Fatigue 23 (6), 509-523.
Walker, K., 1970. The effect of stress ratio during crack propagation and fatigue for 2024-T3 and 7075-T6 aluminum. Effects of environment and complex load history on fatigue life, ASTM STP 462, 1-14.
Wang, X., Masood, S., 2006. Investigation of expansion characteristics of coronary slot stents using finite flement analysis. In: Wang K, Kovacs G, Wozny M, Fang M (eds), Knowledge Enterprise: Intelligent Strategies in Product Design, Manufacturing, and Management, vol 207. IFIP International Federation for Information Processing. Springer Boston, pp. 735-742.
Webb, J.G., 2008. Percutaneous Aortic Valve Replacement Will Become a Common Treatment for Aortic Valve Disease. Journal of the American College of Cardiology: Cardiovascular Interventions 1 (2), 122-126.
Williams, M., 1952. Stress singularities resulting from various boundary conditions in angular corners of plates in extension. J appl Mech 19 (4), 526-528.
Zhi, Y., Wang, X., Gao, Z., Liu, Y., Yue, Z., 2008. Mechanical property analysis of Nitinol defective stent under uniaxial loading/unloading. Materialwissenschaft und Werkstofftechnik 39 (7), 479-485.

Figure Legends

Table 1 Comparison of stent performances. *R* cell from (Kleinstreuer et al. 2008).

Figure 1: Commercially available stents developed for prescribed applications.

Figure 2: Schematic view of the proposed G^2-continuous cell geometry: (a) the proposed E cell geometry; (b) Parameterization required for the synthesis of a G^2-continuous cell shape; (c) inner boundaries of initial design and structurally optimized *E* cell.

Figure 3: a) Schematic view of Nitinol stress-strain curve; b) material constants used in the present study (Kleinstreuer et al. 2008)

Figure 4: Structurally optimized stent. (a) a straight row of lattice cells, (b) a row folded into a cylinder.

Figure 5: FEA results for *E* cell geometry. (a) Strain distribution in the shrunk stent; (b) first principal strain in the stent after stent deployment under 100 mm-Hg mean pressure.; (c) von Mises stress (in MPa) distribution in the artery after stent deployment under 100 mm-Hg mean pressure. The maximum value occurs at the interface between stent and artery wall.

Figure 6: Radial supportive force versus stent outer diameter of *E*-stents compared to *R* cell stent (Kleinstreuer et al. 2008) for a given area in contact with the artery wall. The design parameters for *E*-stent are n_c=8, n_l=10, t=0.28*mm*, w=0.45*mm*, while those for *R* stent are n_c=20, n_l=10, t=0.28*mm*, w=0.35*mm* (Kleinstreuer et al. 2008).

Figure 7: Plots of number of cells in the circumferential and radial direction, thickness and width of cell elements versus radial force, fatigue safety factor, and metal area in contact with artery for *E* cell geometry. (a-c) effect of n_c for , n_l=10,t=0.28*mm*, w=0.45*mm* (d-f) effect of n_l for t=0.28*mm*, w=0.45*mm* , n_c=8; (g-i) effect of t for, w=0.45*mm* , n_l=10, n_c=8; (j-l) effect of w for, t=0.28*mm* , n_l=10, n_c=8 for *E* cell geometries. *R* stent is a benchmark stent design (Kleinstreuer et al. 2008); its design parameters are n_c=20, n_l=10, t=0.28*mm*, w=0.35*mm*.

Figure 1

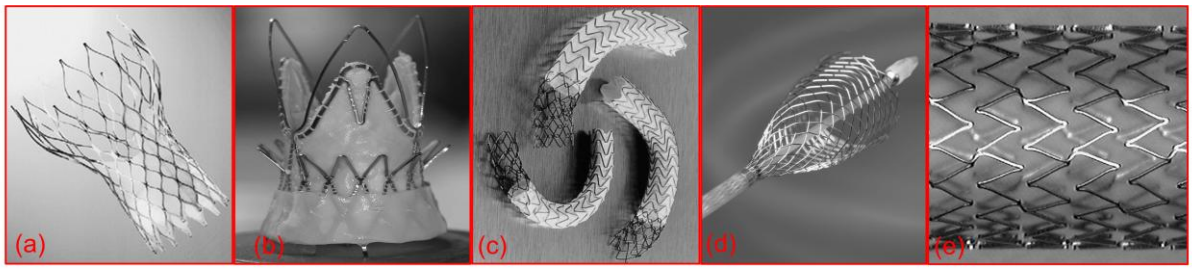

The self-expanding CoreValve (CoreValve Inc.,Irvine, California) (Webb 2008)

The Symetis W aortic stent Valve (Symetis, Lausanne, Switzerland) (Vergnat et al. 2009)

Viatorr stent-graft (WL Gore, Flagstaff, AZ) (Rose et al. 2001)

Wallstent Cobalt SE stent (Boston Scientific Boston USA) Original picture from: http:// bostonscientific.mediaroom.

SMART Nitinol SE stent (Cordis, Florida, USA) (Cordis S.M.A.R.T.™ Control, Nitinol Stent System)

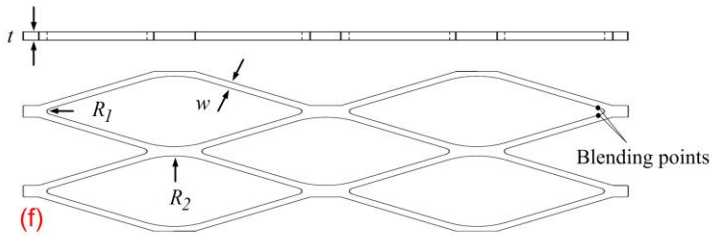

Schematic view of the available diamond-cell stent geometry (a) front view (b) top view (Zhi et al. 2008)

Fig. 1. Commercially available stents developed for prescribed applications.

Figure 2

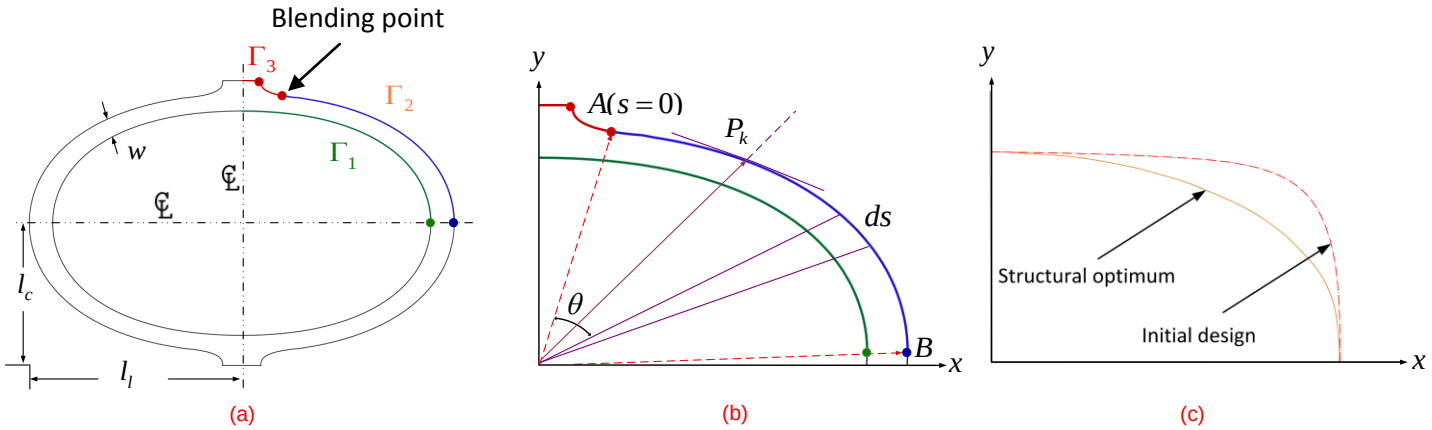

Fig. 2. Schematic view of the proposed G^2-continuous cell geometry: (a) the proposed E cell geometry; (b) Parameterization required for the synthesis of a G^2-continuous cell shape; (c) inner boundaries of initial design and structurally optimized *E* cell.

Figure 3

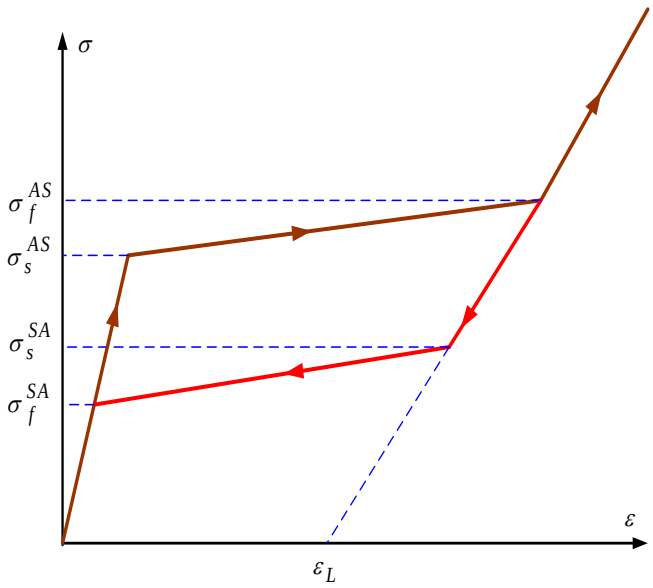

Martensit phase Young modulus	*47.8GPa*
Austenite phase Young modulus	*51.7GPa*
ν	*0.3*
σ_s^{AS}	*600MPa*
σ_f^{AS}	*670MPa*
σ_s^{SA}	*288MPa*
σ_f^{SA}	*254MPa*
ε_L	*6.3%*

Fig. 3. a) Schematic view of Nitinol stress-strain curve; b) material constants used in the present study (Kleinstreuer et al. 2008)

Figure 4

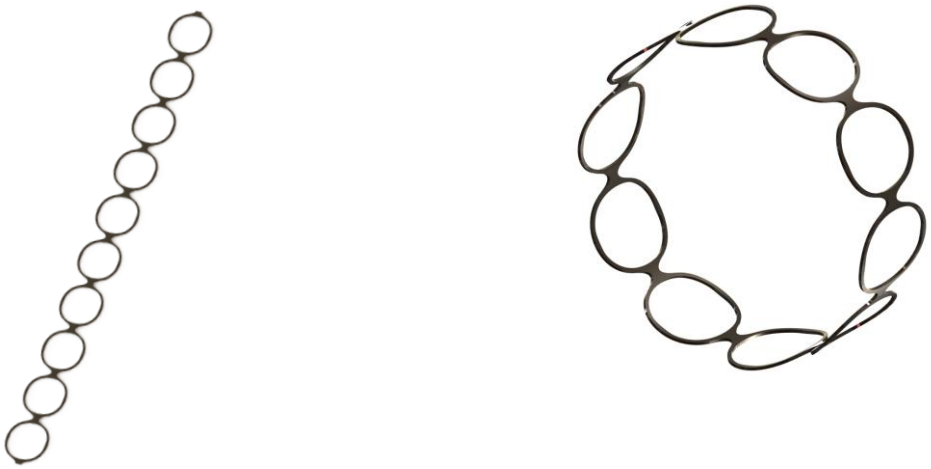

Fig. 4. Structurally optimized stent. (a) a straight row of lattice cells, (b) a row folded into a cylinder.

Figure 5

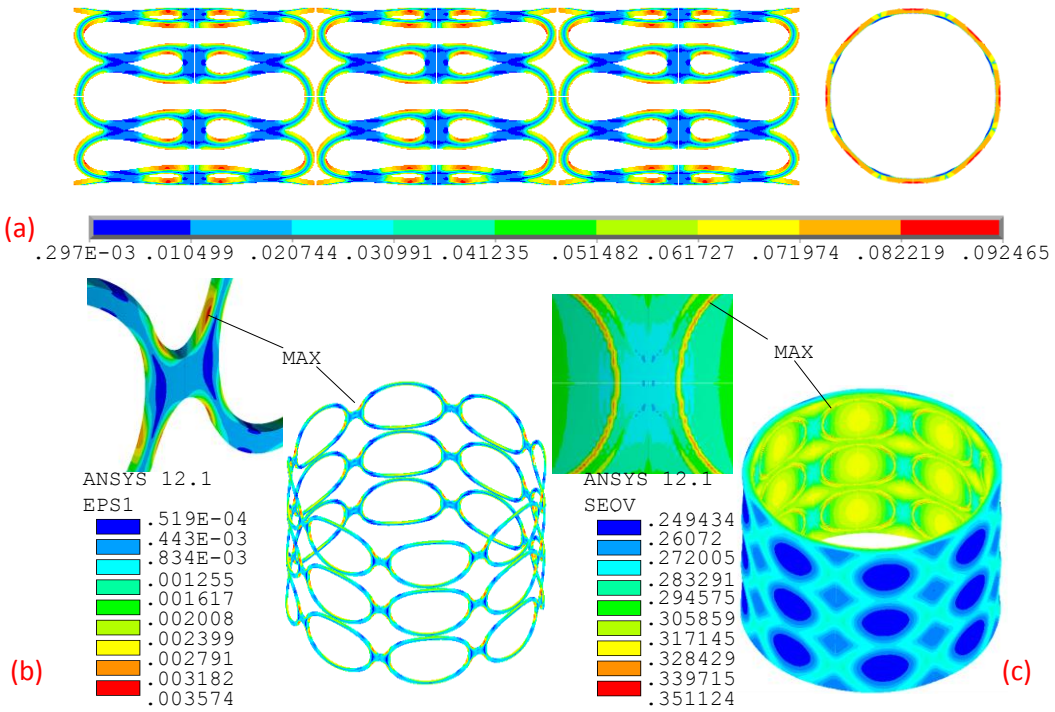

Fig. 5. FEA results for *E* cell geometry. (a) Strain distribution in the shrunk stent; (b) first principal strain in the stent after stent deployment under 100 mm-Hg mean pressure.; (c) von Mises stress (in MPa) distribution in the artery after stent deployment under 100 mm-Hg mean pressure. The maximum value occurs at the interface between stent and artery wall.

Figure 6

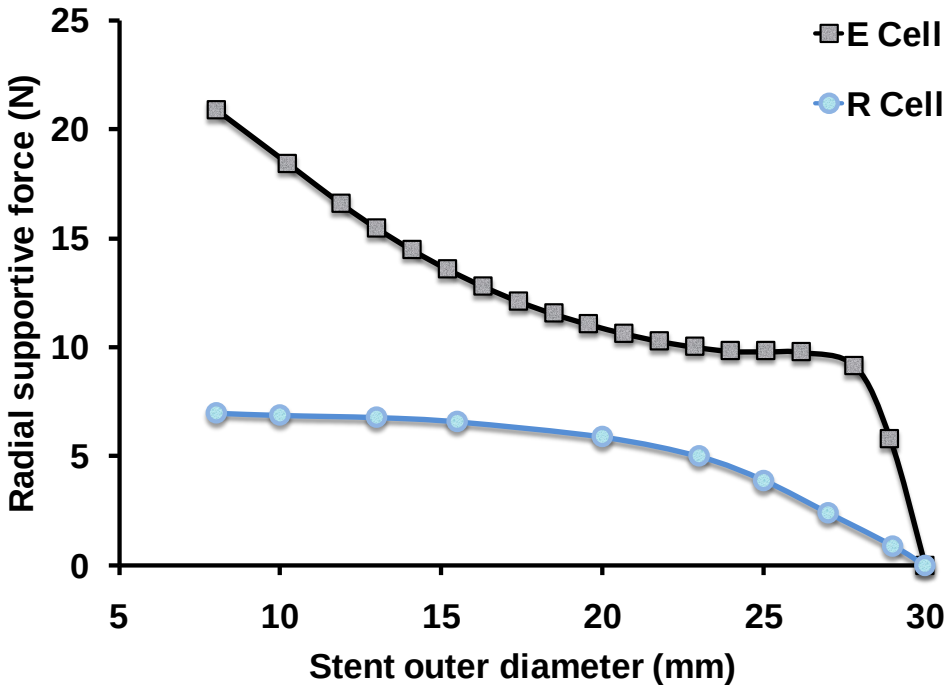

Fig. 6. Radial supportive force versus stent outer diameter of *E*-stents compared to *R* cell stent (Kleinstreuer et al. 2008) for a given area in contact with the artery wall. The design parameters for *E*-stent are n_c=8, n_l =10, t=0.28*mm*, w=0.45*mm*, while those for *R* stent are n_c=20, n_l =10, t=0.28*mm*, w=0.35*mm* (Kleinstreuer et al. 2008).

Figure 7

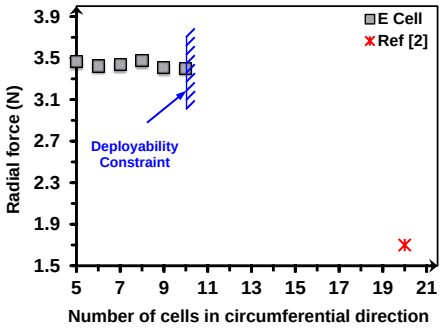

(a)

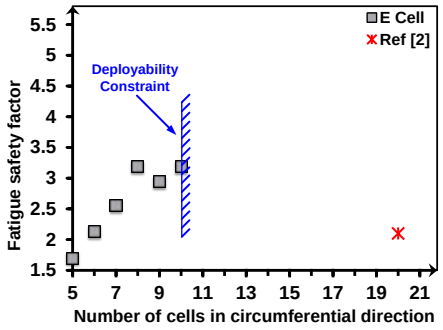

(b)

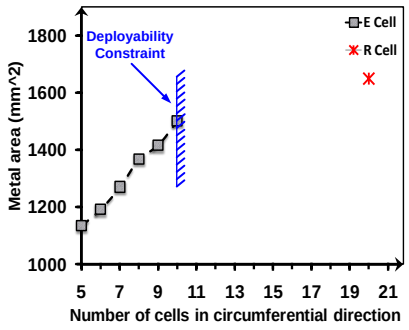

(c)

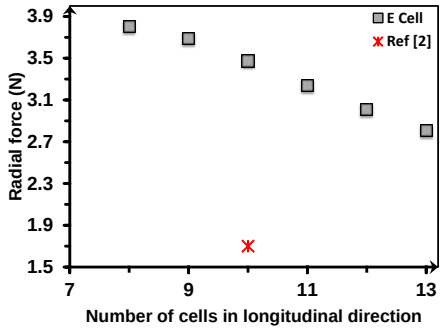

(d)

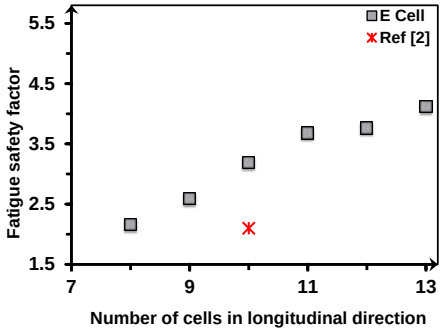

(e)

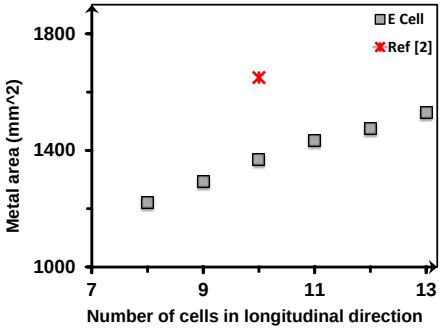

(f)

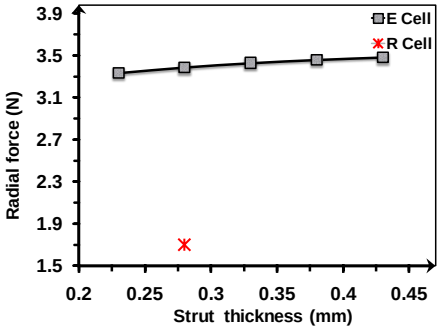

(g)

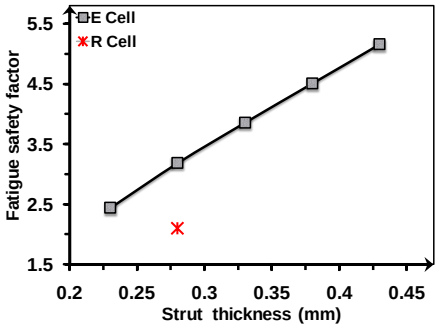

(h)

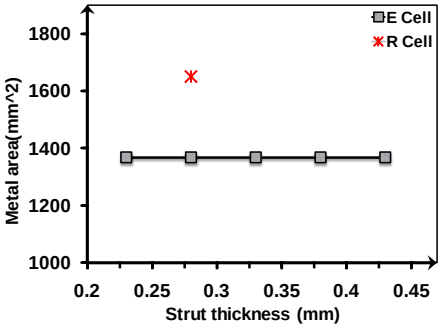

(i)

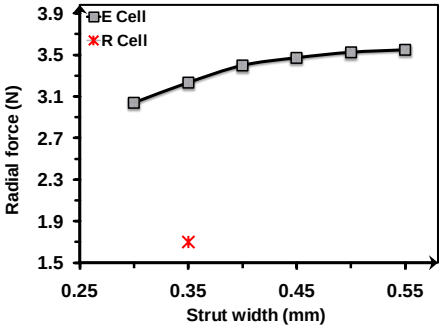

(j)

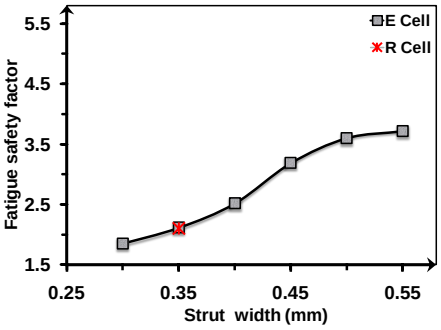

(k)

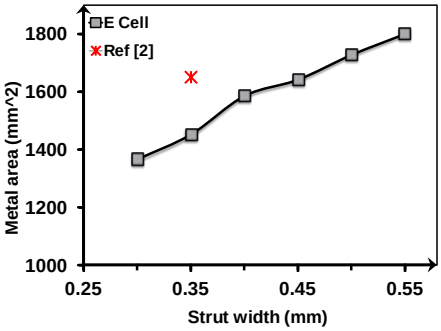

(l)

Fig. 7. Plots of number of cells in the circumferential and radial direction, thickness and width of cell elements versus radial force, fatigue safety factor, and metal area in contact with artery for *E* cell geometry. (a-c) effect of n_c for , n_l =10,*t*=0.28*mm*, *w*=0.45*mm* (d-f) effect of n_l for *t*=0.28*mm*, *w*=0.45*mm* , n_c=8; (g-i) effect of *t* for, *w*=0.45*mm* , n_l =10, n_c=8; (j-l) effect of *w* for, *t*=0.28*mm* , n_l =10, n_c=8 for *E* cell geometries. *R* stent is a benchmark stent design (Kleinstreuer et al. 2008); its design parameters are n_c=20, n_l =10, *t*=0.28*mm*, *w*=0.35*mm*.

Table 1

Table 1 Comparison of stent performances. *R* cell from (Kleinstreuer et al. 2008).

	Radial force at 100 *mmHg* (N)	Fatigue safety factor	Wall stress (MPa)	Maximum shrunk strain (%)
***E* cell**	3.1	3.4	0.351	9.42
***R* cell**	1.7	2.01	0.265	8.86

Conflict of interest Statement

There are no conflicts of interest in this study.